Materials Research Express

PAPER • OPEN ACCESS

Wideband dielectric properties of silicon and glass substrates for terahertz integrated circuits and microsystems

To cite this article: Nonchanutt Chudpooti *et al* 2021 *Mater. Res. Express* **8** 056201

View the article online for updates and enhancements.

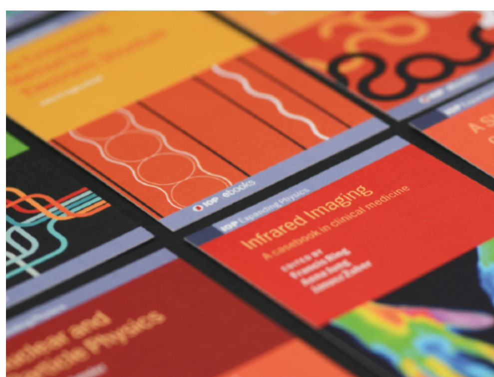

IOP ebooks™

Bringing together innovative digital publishing with leading authors from the global scientific community.

Start exploring the collection–download the first chapter of every title for free.

This content was downloaded from IP address 51.241.127.84 on 16/08/2021 at 16:15

Materials Research Express

OPEN ACCESS

RECEIVED
26 January 2021

REVISED
30 March 2021

ACCEPTED FOR PUBLICATION
9 April 2021

PUBLISHED
26 May 2021

Original content from this work may be used under the terms of the Creative Commons Attribution 4.0 licence.

Any further distribution of this work must maintain attribution to the author(s) and the title of the work, journal citation and DOI.

PAPER

Wideband dielectric properties of silicon and glass substrates for terahertz integrated circuits and microsystems

Nonchanutt Chudpooti[1], **Nattapong Duangrit**[2], **Andrew D Burnett**[3], **Joshua R Freeman**[4], **Thomas B Gill**[4], **Chuwong Phongcharoenpanich**[1], **Ulrik Imberg**[5], **Danai Torrungrueng**[6], **Prayoot Akkaraekthalin**[7], **Ian D Robertson**[4] and **Nutapong Somjit**[4]

[1] School of Engineering, King Mongkut's Institute of Technology Ladkrabang, Bangkok 10520, Thailand
[2] Faculty of Engineering, Rajamangala University of Technology Lanna, Chiang Mai 50300, Thailand
[3] School of Chemistry, University of Leeds, Leeds LS2 9JT, United Kingdom
[4] School of Electronic and Electrical Engineering, University of Leeds, Leeds LS2 9JT, United Kingdom
[5] Huawei Technologies Sweden AB, 164 40 Kista, Sweden
[6] Research Center of Innovation Digital and Electromagnetic Technology (iDEMT), Faculty of Technical Education, King Mongkut's University of Technology North Bangkok, Bangkok 10800, Thailand
[7] Faculty of Engineering, King Mongkut's University of Technology North Bangkok, Bangkok 10800, Thailand

E-mail: c.nonchanutt@gmail.com

Keywords: THz time-domain spectroscopy, material characterization, dielectric properties, electrical properties

Abstract

This paper presents a comprehensive study of the optical and electrical dielectric material properties of six commonly-used silicon and glass substrates at terahertz (THz) frequencies, including refractive index, absorption coefficient, dielectric constant and loss factor. The material characterization techniques used in this paper feature THz time-domain transmission and reflection spectroscopy with the measurement frequencies from 0.5 THz up to a maximum of 6.5 THz. Of the six selected dielectric and semiconductor substrates, two are silicon wafers with resistivities ranging from 0.001 to 0.02 Ω-cm. From the measurement results, loss tangents of the selected silicon wafers range from 0.680 to 5.455 and the dielectric constants are from 1.079 to 17.735. The four other wafers are all glass-based substrates: D263 glass, Borofloat 33 glass, fused silica and Sapphire. From the measurements, it is found that the THz dielectric properties vary considerably between the substrate samples e.g. dielectric constants range from 1.925 to 3.207 while loss tangents are from 0.042×10^{-3} to 0.127. Most of the selected silicon and glass-based substrates are quite useful for many THz applications, e.g., THz integrated circuits (THz ICs), THz microsystem technologies (THz MSTs) and THz system-on-a-chip (THz SoC) and system-on-substrate (SiP).

1. Introduction

Terahertz (THz) research activities have grown significantly over the last few decades with many useful applications including wireless communications [1–4], real- time and high-resolution imaging [5], material characterization [6], space communications [7, 8], as well as chemical and biomedical sensor technologies [9, 10]. As an example, the THz frequency spectrum provides many advantages over RF and microwave bands such as large available bandwidth and high data rate that can achieve multiple terabit-per-second channels for short and medium-range wireless communications, which are very useful for many future scientific and engineering applications. Even though THz technologies can be potentially used for a wide range of applications, most of the state-of-the-art THz components and systems that have been reported in research papers and commercially launched on to the market to-date are often bulky and expensive [2].

Nowadays, many world-leading researchers are moving their research activities toward integrated circuits (ICs), system-on-chip (SoC) and system-in-package (SiP) at THz frequencies using silicon and glass technologies. The THz integrated circuits (THz ICs) and THz micro-electromechanical systems (THz MEMS) that can operate from 100 GHz and up to several hundreds of gigahertz [10–25]. Silicon, such as CMOS and

© 2021 The Author(s). Published by IOP Publishing Ltd

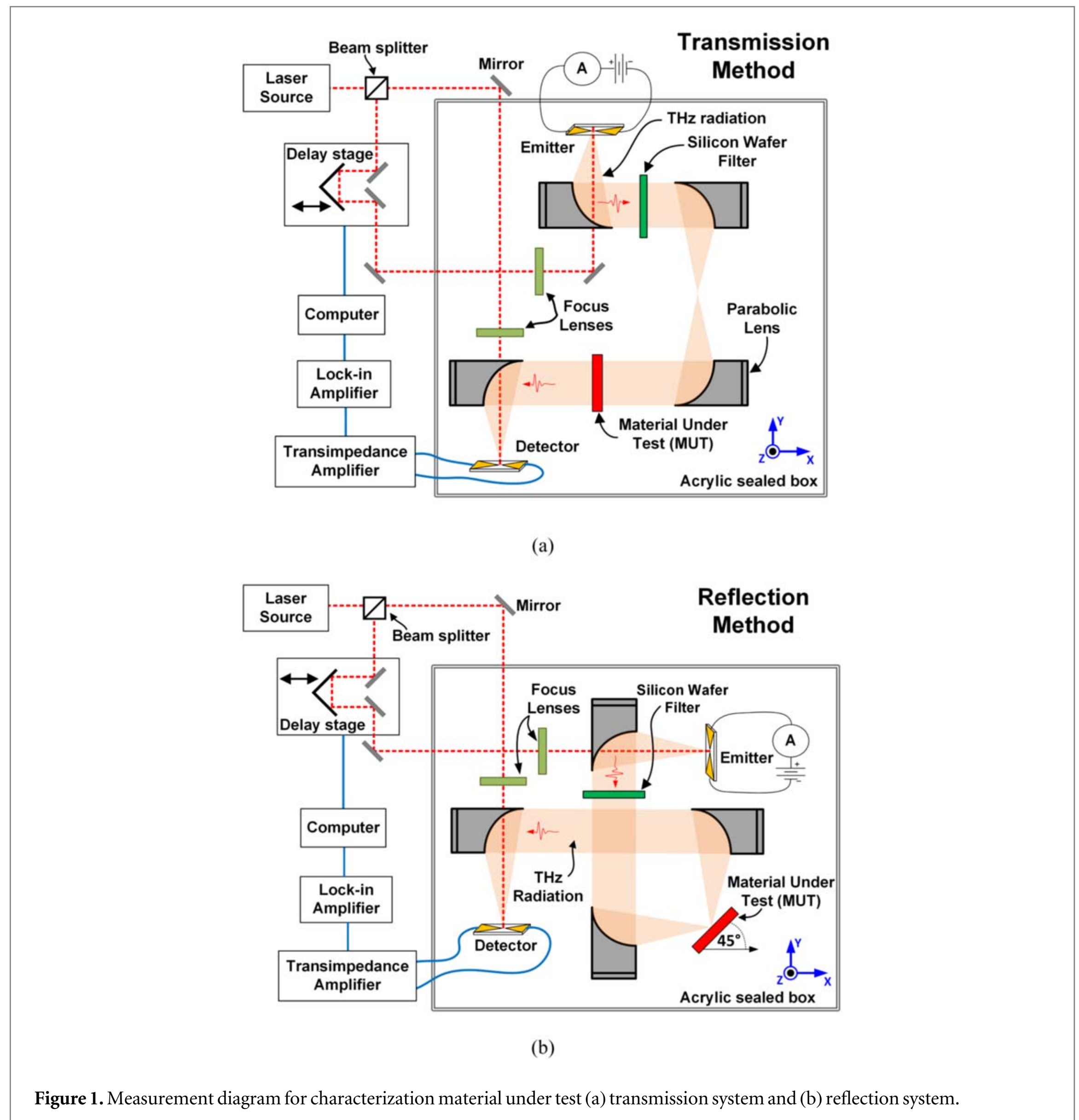

Figure 1. Measurement diagram for characterization material under test (a) transmission system and (b) reflection system.

Table 1. List of selected wafers used in this work.

Wafer material	Wafer type	Dopant	Orientation	Polish*	Wafer diameter (mm/inch)	Wafer thickness (μm)	Resistivity (Ω cm)
Silicon	N-type	Phosphorous (P)	⟨100⟩	SSP	100/4	500	0.001–0.005
Silicon	P-type	Boron (B)	⟨100⟩	SSP	100/4	525	0.010–0.020
D263 glass	—	—	—	DSP	100/4	500	—
Fused Silica	—	—	—	DSP	100/4	500	—
Borofloat 33 glass	—	—	—	DSP	100/4	500	—
Sapphire	—	—	C Plane	DSP	100/4	600	—

*SSP is Single Side Polish
DSP is Double Side Polish

BiCMOS, and glass-based technologies are good candidates for THz circuits and systems since they are able to provide a high level of integration with consumer electronics, offering great potential to integrate THz systems onto a single chip or substrate [3, 21–26]. They can also achieve high yield at low fabrication cost for mass production, which is needed to decrease overall production cost per unit while still achieving excellent performance compared to their compound semiconductor counterparts such as GaAs and InP technologies. However, the lack of comprehensive data for the substrate material properties, such as dielectric constant, loss

tangent and absorption coefficient, at THz frequencies above one THz drastically limits the usability of silicon and glass-based technologies. Currently, there are some research works reporting on both optical and electrical dielectric properties of only a few different glass and silicon substrates for a maximum frequency of up to approximately 3 THz [26–39].

This paper presents the comprehensive dielectric material properties in both optical and electrical domains, such as dielectric constant, loss tangent and absorption coefficient, of six commonly-used silicon and glass substrates, measured using THz time-domain spectroscopy (THz TDS) over a frequency range from 0.5 THz to 6.5 THz. The important material information of the selected silicon and glass substrates such as crystal orientation, substrate resistivity, doping level, etc are summarized in table 1. Both transmission and reflection THz spectroscopy techniques were used to characterize the selected substrates depending on the relevance to the wafer samples, e.g. substrate thickness, wafer diameter and material resistivity. This characterization of dielectric material parameters is a significant step in the development of various integrated passive and active THz components for THz ICs, THz MST and THz SoC/SiP devices.

2. THz time-domain spectroscopy systems

Figures 1 (a), (b) shows the schematic diagrams of the transmission and reflection measurement systems, respectively. The working principle and measurement setup of the free-space THz-TDS systems have been reported previously [31, 40–45]. The choice between transmission and reflection measurement depends on the physical and dielectric properties of the material-under-test (MUT), e.g. thickness and loss levels of the MUT. Transmission measurements are suitable for characterizing most substrate materials, which are generally thin samples of

low-attenuation dielectric or semiconductor materials. The main advantage of the transmission technique is the ease with which distinct absorption peaks can be observed in the response during the material measurement, either in refractive index or dielectric constant. Transmission measurements can achieve very accurate results for the extracted material parameters.

However, the transmission technique is not suitable for thick samples of dielectric and semiconductor materials, or for materials-under-test with high signal attenuation [42, 43, 45]. In these cases, the reflection method is preferable. Rather than pre-judge the results, both the transmission and reflection techniques were used in this work as complementary material characterization methods providing a complete set of MUT data. The measurement system gives highly accurate results and provides quick indication of the properties of the six wafers with a better than 93% accuracy. The standard deviation of the measurement system is lower than 0.0271. However, due to high absorption of some of the MUT samples in this work, the extracted dielectric and optical properties for some materials cannot be reported over the whole frequency band of 0.5 to 6.5 THz.

2.1. Transmission and reflection measurement setup

The transmission and reflection TDS systems were based on established optical bench setups in the Terahertz Laboratories of the Pollard Institute at Leeds. A commercial mode-locked Ti:Sapphire laser (Coherent Vitara-T-HP) operating at 800 nm was employed, set to a repetition rate of 80 MHz, pulse width of 20 fs and with an average power of up to ~1 W [46]. The THz emitter and detector are both photoconductive antennas (PCA), comprising two bow-tie shaped Ti:Au electrodes with a 200 μm gap between them, deposited on low-temperature-grown GaAs (LT-GaAs) and transferred onto z-cut quartz substrate [40]. In both the transmission and reflection setups, the laser output is split into two beams using an 80:20 beam splitter. The higher power beam is fed to one PCA to generate the THz pulse, while the weaker beam is fed to the other PCA for gated detection of the THz signal received from the sample. The signal generation PCA is biased at 350 V and electrically chopped at 7 kHz, and the resulting THz radiation is then collected, collimated and re-focused by a set of off-axis parabolic mirrors. A silicon wafer is used as a filter to block any stray laser light reflected from the emitter surface from reaching the detector, while allowing the majority of the THz radiation to pass through.

In the transmission system, shown in figure 1(a), the THz radiation is collected by a second set of off-axis parabolic mirrors and focused onto the PCA detector. Before the material under test (MUT) is inserted, a reference 'thru' measurement is made. Then, the sample is measured by placing it centrally in the 2-inch collimated THz beam that is formed between this second set of off-axis parabolic mirrors. In the reflection measurement setup, shown in figure 1(b), the THz radiation is focused onto the sample, which is set at a 45° angle of incidence, using parabolic mirrors. A second pair of parabolic mirrors is used to re-collimate the reflected THz signal and focus it onto the PCA detector. A reference measurement was performed using a large area of Ti:Au conductor (100 nm thick, deposited on the same wafer) as a reflection standard.

In both setups, the 800 nm laser beam is focused onto the PCA detector through a hole in the final parabolic mirror. Only when both the laser pulse and THz radiation are incident on the detector, can the THz field at that

point in time be measured. A linear delay stage is, therefore, used to synchronize the optical and THz pulses at the detector and ensure that the full THz electric field is sampled. The output signal from the PCA detector is first amplified using a transimpedance amplifier and then measured using a lock-in amplifier referenced to the bias frequency of the THz PCA emitter. The THz part of the system is enclosed in a Perspex box so that it can be purged with dry air to a humidity of $<1\%$. This is important in order to remove water vapor absorption effects from the measured data.

2.2. Material characterization extraction

Free-space THz-TDS is now the most common technique to characterize material properties at THz frequencies. Both the amplitude and phase of the measurement signal are collected simultaneously and can be used to extract both the optical properties, e.g., refractive index and absorption coefficient, or the electrical properties, e.g. dielectric constant and loss factor of the MUT. The complex refractive index, $\tilde{n}(\omega)$, can be related to the complex permittivity, $\tilde{\varepsilon}(\omega)$, via the mathematical relation $(\tilde{n}(\omega))^2 = \tilde{\varepsilon}(\omega)$, where ω is the angular frequency [47, 48].

The, $\tilde{S}_{sample}(\omega)$, and reference, $\tilde{S}_{ref}(\omega)$, scans are recorded independently and transformed from the time domain to the frequency domain by using a Fourier transform. The ratio of $\tilde{S}_{sample}(\omega)$ and $\tilde{S}_{ref}(\omega)$ are represented by the magnitude, $\rho(\omega)$, and phase, $\phi(\omega)$ [49], as follows:

$$\frac{\tilde{S}_{sample}(\omega)}{\tilde{S}_{ref}(\omega)} = \rho(\omega)\cdot e^{-j\phi(\omega)} \tag{1}$$

From equation (1), the refractive index, $n_{sample}(\omega)$, and extinction coefficient, $k_{sample}(\omega)$, of the MUT can be represented as follows:

$$n_{sample}(\omega) = \phi(\omega)\cdot\frac{c_{vacuum}}{d} + 1 \tag{2}$$

and

$$k_{sample}(\omega) = \ln\left(\frac{4\cdot n_{sample}(\omega)}{\rho(\omega)\cdot(n_{sample}(\omega)+1)^2}\right)\cdot\frac{c_{vacuum}}{\omega\cdot d} \tag{3}$$

where c_{vacuum} is the velocity of light in vacuum and d is thickness of the wafer in centimeters. The extinction coefficient, $k_{sample}(\omega)$, can be calculated in terms of the absorption coefficient, α, as follows:

$$k_{sample}(\omega) = \frac{\alpha(\omega)\cdot c_{vacuum}}{2\cdot\omega} \tag{4}$$

and

$$\alpha(\omega) = \frac{2}{d}\cdot\ln\left(\frac{4\cdot n_s(\omega)}{\rho(\omega)\cdot(n_{sample}(\omega)+1)^2}\right) \tag{5}$$

The complex permittivity can be represented by $\tilde{\varepsilon}(\omega) = \varepsilon'(\omega) - j\cdot\varepsilon''(\omega)$, where the real and imaginary parts are $\varepsilon'(\omega)$ and $\varepsilon''(\omega)$, respectively. The real part, $\varepsilon'(\omega)$, and imaginary part, $\varepsilon''(\omega)$, of the complex permittivity are expressed by:

$$\varepsilon'(\omega) = (n_{sample}(\omega))^2 - (k_{sample}(\omega))^2 \tag{6}$$

and

$$\varepsilon''(\omega) = 2\cdot n_{sample}(\omega)\cdot k_{sample}(\omega) \tag{7}$$

For the electrical properties, the dielectric constant is equal to the real part of the permittivity, $\varepsilon'(\omega)$ and the loss tangent can be calculated as follows:

$$\tan\delta = \frac{\varepsilon''(\omega)}{\varepsilon'(\omega)} = \frac{2\cdot n_{sample}(\omega)\cdot k_{sample}(\omega)}{(n_{sample}(\omega))^2 - (k_{sample}(\omega))^2} \tag{8}$$

3. Measurement results

Table 1 lists the selected semiconductor and dielectric substrates to be characterized, which are commonly used in ICs, MSTs and SoC/SiPs, with their relevant detailed information e.g. names and types of material, level of dopant, substrate thickness and diameter, and substrate resistivity. All the selected substrates [50], have a substrate diameter of 100 mm that fits in a 4-inch optics holder. Before mounting the substrate-under-test in the holder, the tested wafer was cleaned to remove both organic and inorganic contaminations by dipping it firstly

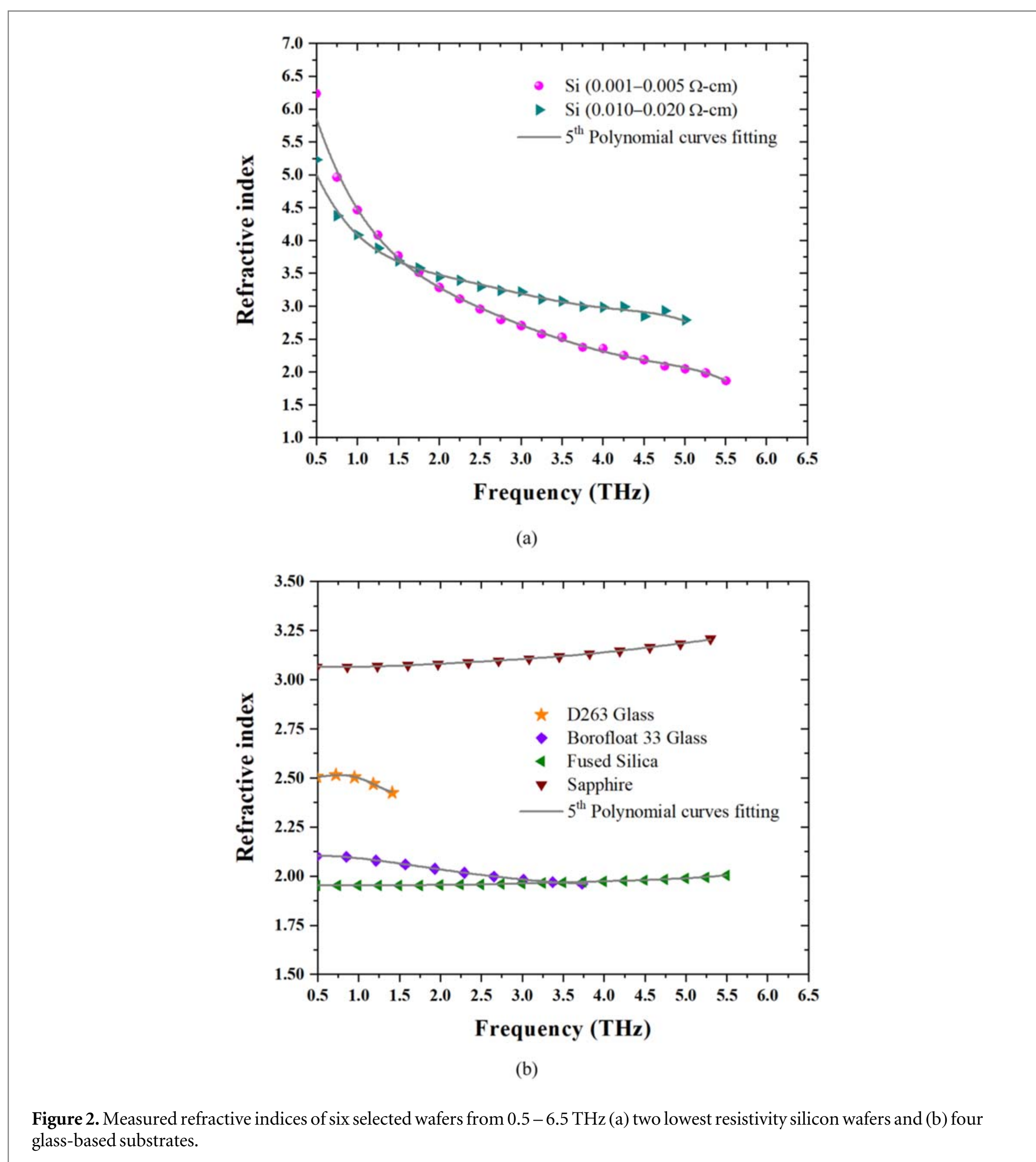

Figure 2. Measured refractive indices of six selected wafers from 0.5 – 6.5 THz (a) two lowest resistivity silicon wafers and (b) four glass-based substrates.

into acetone and then isopropyl alcohol and immediately rinsing in deionized water before drying it in a clean environment at room temperature using laboratory-grade dry compressed air. Individual measurements were repeated at least two times to ensure the repeatability. The averages were subsequently used to extract the optical and electrical dielectric material properties of the six commonly-used silicon and glass substrates. Owing to the dynamic range of both THz-TDS instruments, the measurement of either very strongly absorbing or very weakly absorbing samples is difficult. Therefore, for strongly absorbing samples, the data has been truncated at the point that the spectra have intercepted the maximum absorption α_{max} coefficient detectable [51]. For weakly absorbing samples, the data has been truncated at the point that the measured absorption coefficient is indistinguishable from a thru measurement. Therefore, not all samples have data presented across the entire 0.5 to6.5 THz range of the instrument.

3.1. Reflective indices

The refractive indices of all six wafers from 0.5 to 6.5 THz are shown in figure 2. Figure 2(a) shows the refractive indices of the low resistivity silicon wafers, e.g. 0.001–0.005 Ω-cm and 0.01–0.02 Ω-cm. The refractive indices of both wafers decrease dramatically with increasing frequency. The refractive indices of the 0.001–0.005 Ω-cm and 0.01–0.02 Ω-cm silicon wafers at 0.5 THz are 6.23 and 5.22, respectively, while the value decreases to 2.04 and 2.79 at 5.0 THz, respectively. Figure 2(b) depicts the refractive indices of D263 glass, Borofloat 33 glass, fused silica and Sapphire. The refractive indices of fused silica and sapphire slightly increase from 1.95 and 3.06 at 0.5

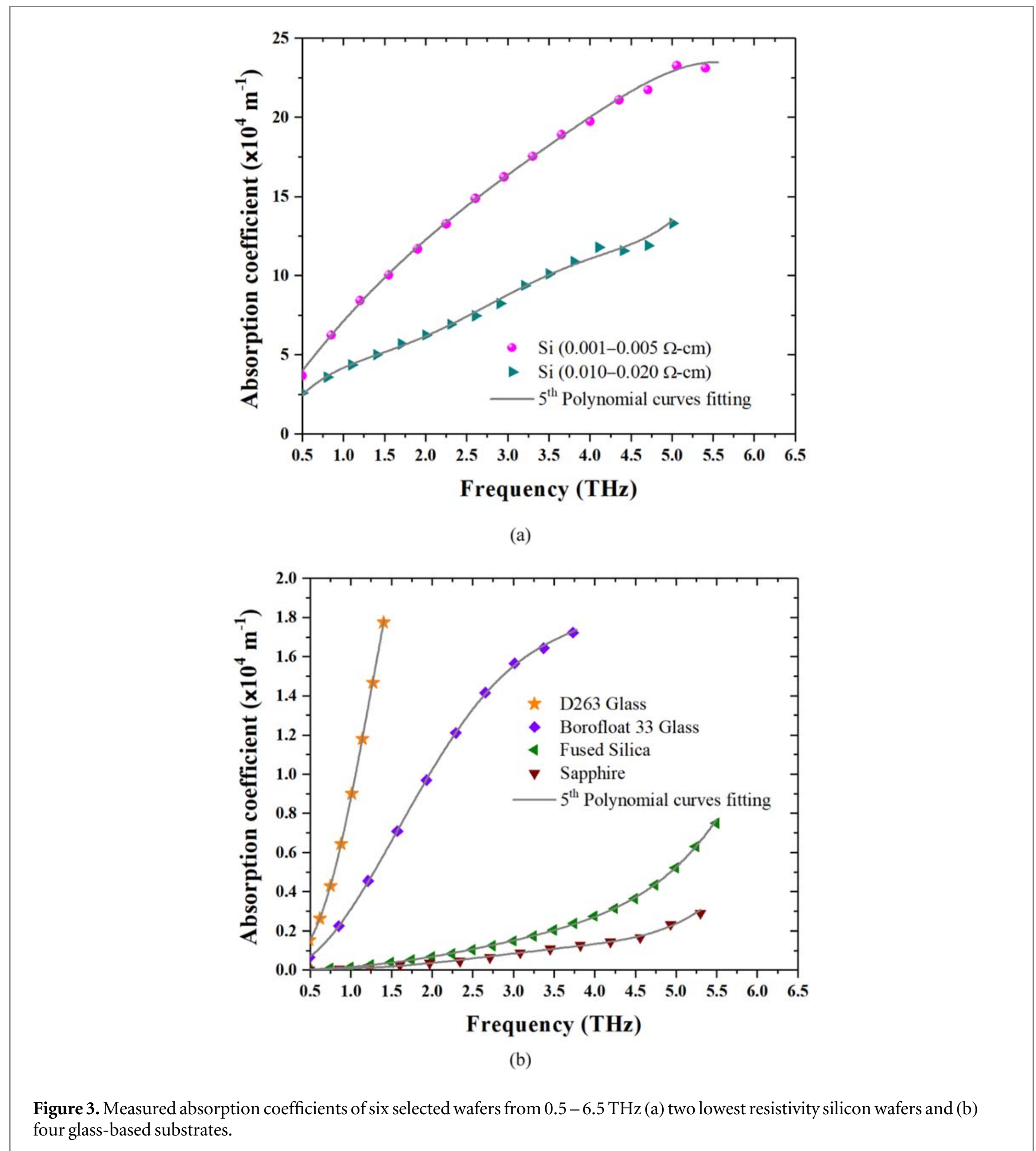

Figure 3. Measured absorption coefficients of six selected wafers from 0.5 – 6.5 THz (a) two lowest resistivity silicon wafers and (b) four glass-based substrates.

THz to 2.00 and 3.20 at 5.3 THz. On the other hand, the refractive indices of D263 glass and Borofloat 33 glass show a decreasing trend with increased frequency. The refractive index of D263 glass decreases from 2.50 at 0.5 THz to 2.42 at 1.4 THz. The refractive index of Borofloat 33 reduces from 2.10 at 0.5 THz to 1.95 at 3.8 THz.

3.2. Absorption coefficients

The absorption coefficients of all six wafers characterized from 0.5 to 6.5 THz are shown in figure 3. The absorption coefficients of the silicon wafers with resistivity 0.001–0.005 Ω-cm and 0.01–0.02 Ω-cm are presented in figure 3(a). The absorption coefficients show an opposite trend to refractive index and dramatically increase as a function of frequency. The absorption coefficients of the 0.001–0.005 Ω-cm and 0.01–0.02 Ω-cm silicon wafers at 0.5 THz are 3.67×10^4 m^{-1} and 2.61×10^4 m^{-1}, respectively, while the value increases to 2.26×10^5 m^{-1} and 1.33×10^5 m^{-1} at 5.0 THz, respectively. Figure 3(b) shows the absorption coefficients of D263 glass, Borofloat 33 glass, fused silica and Sapphire, all of which increase as a function of frequency. The absorption coefficient of D263 glass and Borofloat 33 glass dramatically increase from 1.61×10^3 m^{-1} and 0.682×10^3 m^{-1} at 0.5 THz, respectively, to 1.81×10^4 m^{-1} at 1.4 THz and 1.71×10^4 m^{-1} at 3.8 THz, while the absorption coefficients of the fused silica and Sapphire wafers at 0.5 THz are ~90 m^{-1} and ~12 m^{-1}, and increase to 6.63×10^3 m^{-1} and 2.90×10^3 m^{-1} at 5.3 THz.

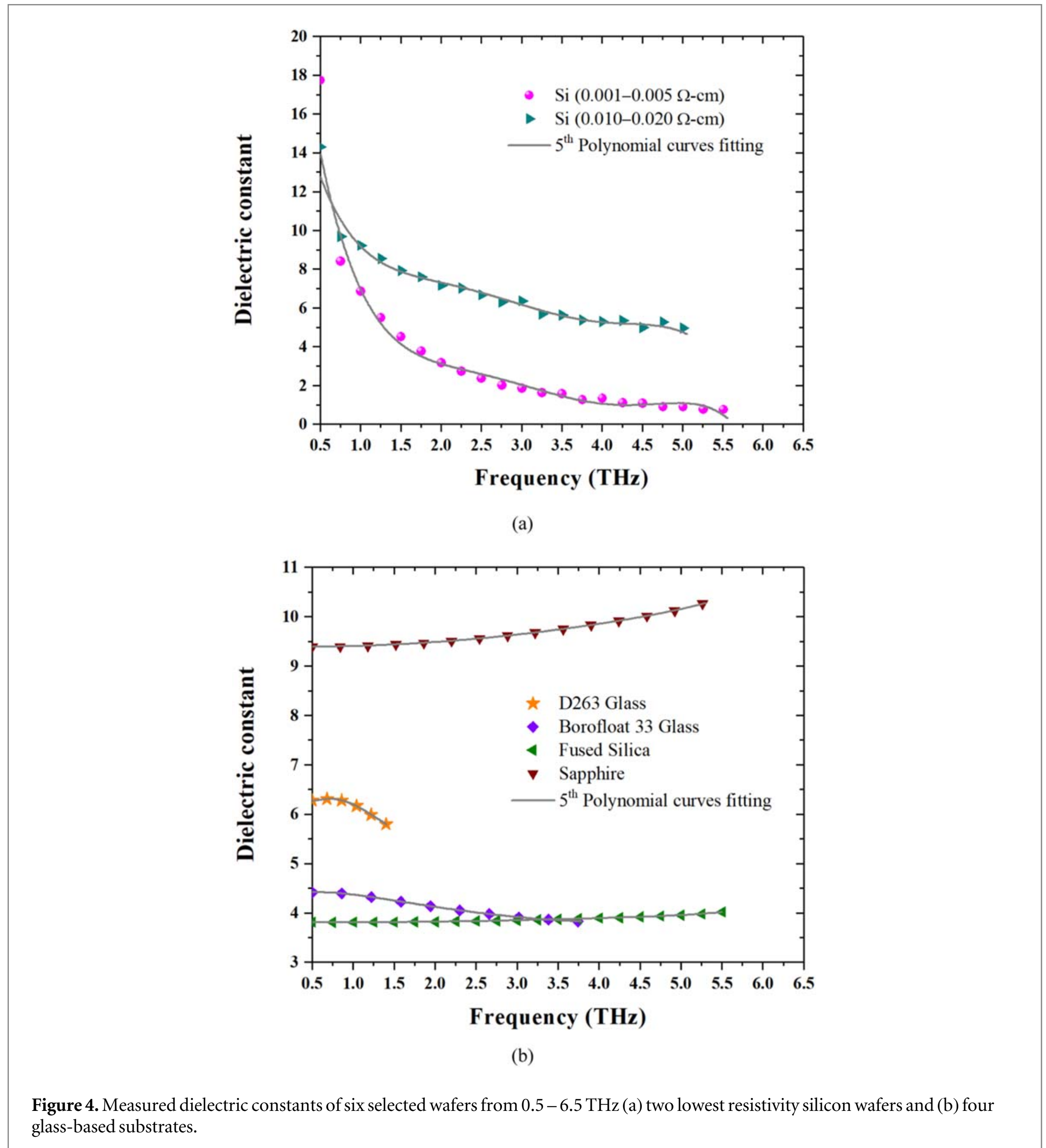

Figure 4. Measured dielectric constants of six selected wafers from 0.5 – 6.5 THz (a) two lowest resistivity silicon wafers and (b) four glass-based substrates.

3.3. Dielectric constants

From the measured refractive indices and absorption coefficients, equation (6) in section II can be used to calculate the dielectric constants of the six selected wafers, and these are shown in figure 4. Figure 4(a) shows the dielectric constants of two lowest resistivity silicon wafers. The dielectric constant of the 0.001–0.005 Ω-cm silicon wafer slightly decreases from 17.73 at 0.5 THz to 0.65 at 5.5 THz. The trend of the dielectric constant of the 0.01–0.02 Ω-cm silicon wafer is similar and slightly decreases between 14.31 and 5.09 from 0.5–5.0 THz. Figure 4(b) shows the dielectric constant of four wafers, e.g. D263 glass, Borofloat 33 glass, fused silica and Sapphire. The dielectric constants of fused silica and sapphire slightly increase from 3.81, 9.39 at 0.5 THz, respectively to 4.01 and 10.28 at 5.3 THz, respectively. On the other hand, the dielectric constants of D263 glass and Borofloat 33 glass decrease as frequency increases. The dielectric constant of D263 glass decreases from 6.27 at 0.5 THz to 5.78 at 1.4 THz. The dielectric constant of Borofloat reduces from 4.41 at 0.5 THz to 3.82 at 3.8 THz.

3.4. Loss tangents

Figures 5 (a) and (b) depict the loss tangents of the six selected wafers, as determined using equation (8). From figure 5 (a), the silicon wafer with resistivity between 0.001–0.005 Ω-cm has a loss tangent that increases from 1.5 to 5.5 as a function of frequency. The silicon wafer with resistivity of between 0.01–0.02 Ω-cm has a loss tangent that decreases slightly from 1 at 0.5 THz to 0.68 at 5.0 THz. Figure 5(b) show the loss tangent of the four non-

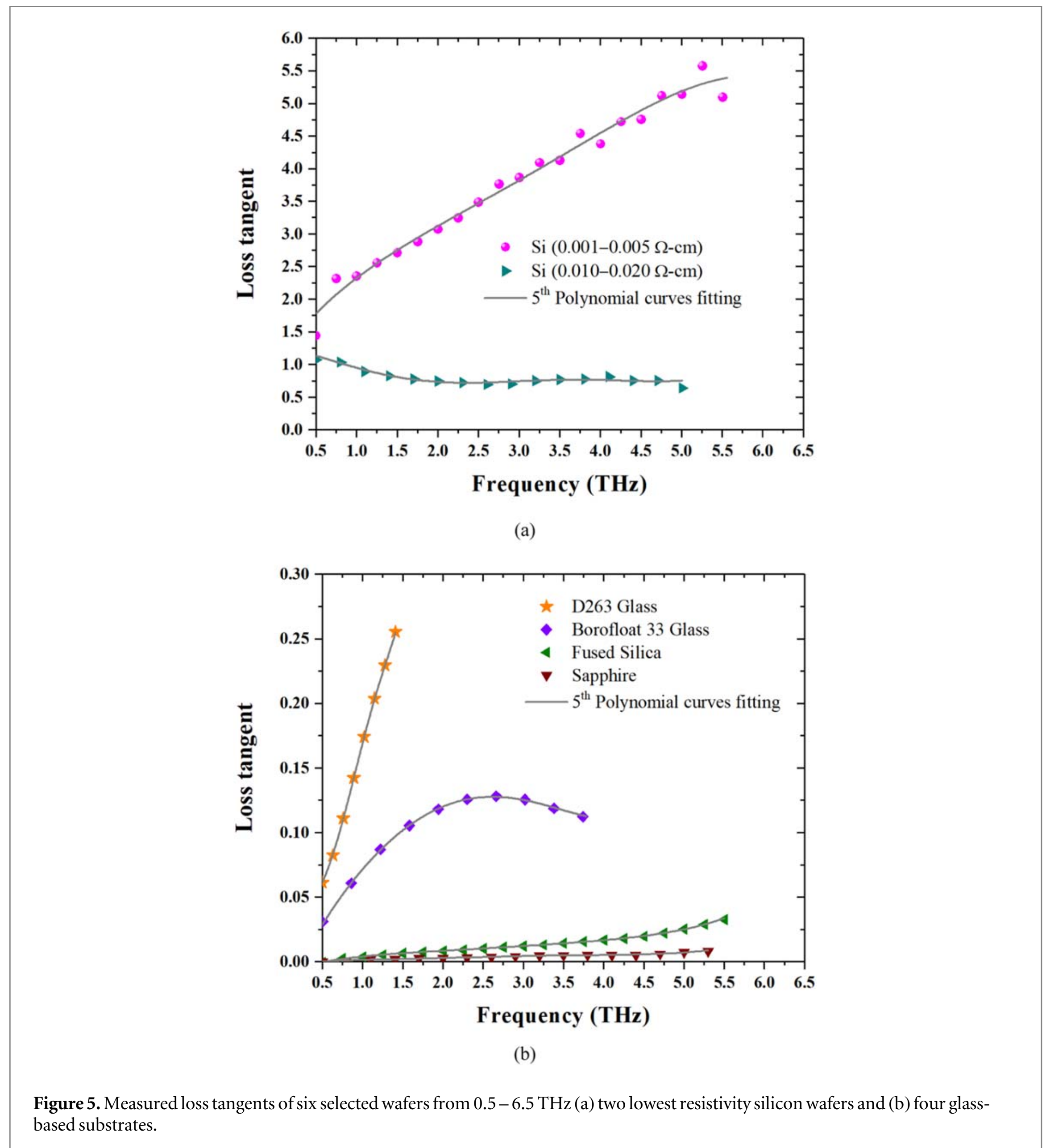

Figure 5. Measured loss tangents of six selected wafers from 0.5 – 6.5 THz (a) two lowest resistivity silicon wafers and (b) four glass-based substrates.

silicon wafers. The loss tangent of D263 glass dramatically increases from 0.059 at 0.5 THz to 0.255 at 1.4 THz. The loss tangent of Borofloat 33 glass increases from 0.031 at 0.5 THz to a maximum value of 0.128 at 2.6 THz before decreasing to 0.11 at 3.8 THz. For the fused silica and Sapphire wafers, the loss tangent increases slightly as a function of frequency. The loss tangents of the fused silica and Sapphire wafers at 0.5 THz are 0.042×10^{-3} and 0.045×10^{-3}, respectively, while the value increases to 0.032 at 5.5 THz and 0.0081 at 5.3 THz, respectively.

3.5. Optical and electrical dielectric properties model

The high fluctuation in the measured data is shown in the data of silicon wafers with resistivities ranging from 0.001 to 0.02 Ω-cm due to the low loss materials. This means the interaction length between the THz beam and the sample is very small and the spectra are dominated by noise. The other problem is the low loss materials tend to lead to multiple reflections in the samples which in turn, lead to large oscillations in the frequency response. To reduce the fluctuation in the measured data, the fluctuation data is filtered out and smoothened by using the commercial data analysis and visualization software package Origin [52], where a 5th order polynomial was used to provide the best fit with the standard deviation lower than 0.0271. The polynomial is given as

$$P(f) = A \cdot f^5 + B \cdot f^4 + C \cdot f^3 + D \cdot f^2 + E \cdot f + F \tag{9}$$

where P(f) is the value of the optical and electrical dielectric properties as a function of frequency f THz. A, B, C, D, E, F are the coefficient of 5th order polynomial function. All values of the coefficient parameters are listed and showed in tables 2–5. The maximum error, average error and average standard deviation of each wafer are

Table 2. Coefficient of 5th polynomial function to perform the refractive index of six wafers.

Wafer material	A	B	C	D	E	F	Maximum %difference (max. error)	Average %difference (avg. error)	Average S.D.
Si ($0.001-0.005\ \Omega$-cm)	−6.3198	3.3997	−1.0071	0.1496	−0.0087	8.2689	6.32	1.01	0.0239
Si ($0.010-0.020\ \Omega$-cm)	−5.2669	3.4028	−1.1432	0.1879	−0.0120	6.9200	5.55	1.14	0.0271
D263 Glass	−1.7638	4.1876	−4.4542	2.1411	−0.3885	2.7753	0.05	0.02	0.0003
Borofloat 33 Glass	0.1289	0.1289	0.0692	−0.0140	0.0011	2.0713	0.11	0.01	0.0002
Fused Silica	0.0109	−0.0134	0.0072	−0.0015	1.1322×10^{-4}	1.9487	0.06	0.02	0.0002
Sapphire	0.0043	−0.0028	0.0041	-8.8541×10^{-4}	7.0834×10^{-5}	3.0621	0.05	0.01	0.0002

Table 3. Coefficient of 5th polynomial function to perform the absorption coefficient of six wafers.

Wafer material	A	B	C	D	E	F	Maximum %Difference (max. error)	Average %Difference (avg. error)	Average S.D.
Si (0.001 − 0.005 Ω-cm)	7.1620×10^{4}	-3.7671×10^{3}	-2.9915×10^{3}	9.8699×10^{2}	−90.6294	5.3951×10^{3}	6.87	1.14	0.0122
Si (0.010 − 0.020 Ω-cm)	1.1504×10^{-5}	-9.0891×10^{4}	3.9389×10^{4}	-7.6814×10^{3}	5.5154×10^{2}	-1.4627×10^{4}	5.11	1.29	0.0136
D263 Glass	7.7188×10^{4}	-1.9645×10^{5}	2.5149×10^{5}	-1.4233×10^{5}	3.0261×10^{4}	-1.1367×10^{4}	1.08	0.28	0.0116
Borofloat 33 Glass	1.3276×10^{3}	2.3306×10^{3}	6.5813×10^{2}	-5.3533×10^{2}	69.3949	-7.0671×10^{2}	2.34	0.75	0.0233
Fused Silica	9.9054×10^{2}	-7.8882×10^{2}	4.4587×10^{2}	-1.012×10^{2}	8.9339	-3.8213×10^{2}	1.81	0.42	0.0107
Sapphire	1.2285×10^{3}	-1.2799×10^{3}	6.7829×10^{2}	-1.5064×10^{2}	12.1517	-3.9132×10^{2}	1.14	0.35	0.0225

Table 4. Coefficient of 5th polynomial function to perform the dielectric constant of six wafers.

Wafer material	A	B	C	D	E	F	Maximum %difference (max. error)	Average %difference (avg. error)	Average S.D.
Si (0.001 − 0.005 Ω-cm)	−40.9394	26.1898	−8.3339	1.2795	−0.0754	28.8499	5.17	1.07	0.0195
Si (0.010 − 0.020 Ω-cm)	−24.0190	17.1995	−6.1566	1.0495	−0.0681	21.1824	4.52	1.27	0.0131
D263 Glass	−9.9821	23.8381	−25.753	12.6283	−2.3424	7.8049	0.11	0.02	0.0009
Borofloat 33 Glass	0.5499	−0.7197	0.3032	−0.0608	0.0049	4.2890	0.21	0.04	0.0012
Fused Silica	0.0439	−0.0535	0.0288	−0.0059	4.4967×10^{-4}	3.7969	0.11	0.02	0.0006
Sapphire	0.0289	−0.0202	0.0261	−0.0057	4.5588×10^{-4}	9.3753	0.10	0.02	0.0012

Table 5. Coefficient of 5th polynomial function to perform the loss tangent of six wafers.

Wafer material	A	B	C	D	E	F	Maximum %Difference (max. error)	Average %Difference (avg. error)	Average S.D.
Si ($0.001 - 0.005\ \Omega$-cm)	1.6839	−0.5319	0.1242	−0.0107	5.8492×10^{-5}	1.0562	3.41	1.27	0.0199
Si ($0.010 - 0.020\ \Omega$-cm)	−0.1585	−0.3661	0.2499	−0.0560	0.0042	1.2746	1.74	0.32	0.0178
D263 Glass	0.5781	−1.5807	2.4138	−1.5535	0.3597	−0.0482	0.91	0.26	0.0002
Borofloat 33 Glass	0.1337	−0.0392	0.0084	−0.0024	3.0026×10^{-4}	−0.0293	0.58	0.13	0.0003
Fused Silica	0.0203	−0.0120	0.0042	-7.4699×10^{-4}	5.3799×10^{-5}	−0.0079	0.77	0.14	0.0002
Sapphire	0.0064	−0.0049	0.0023	-4.9485×10^{-4}	3.9241×10^{-5}	−0.0019	0.43	0.11	0.0002

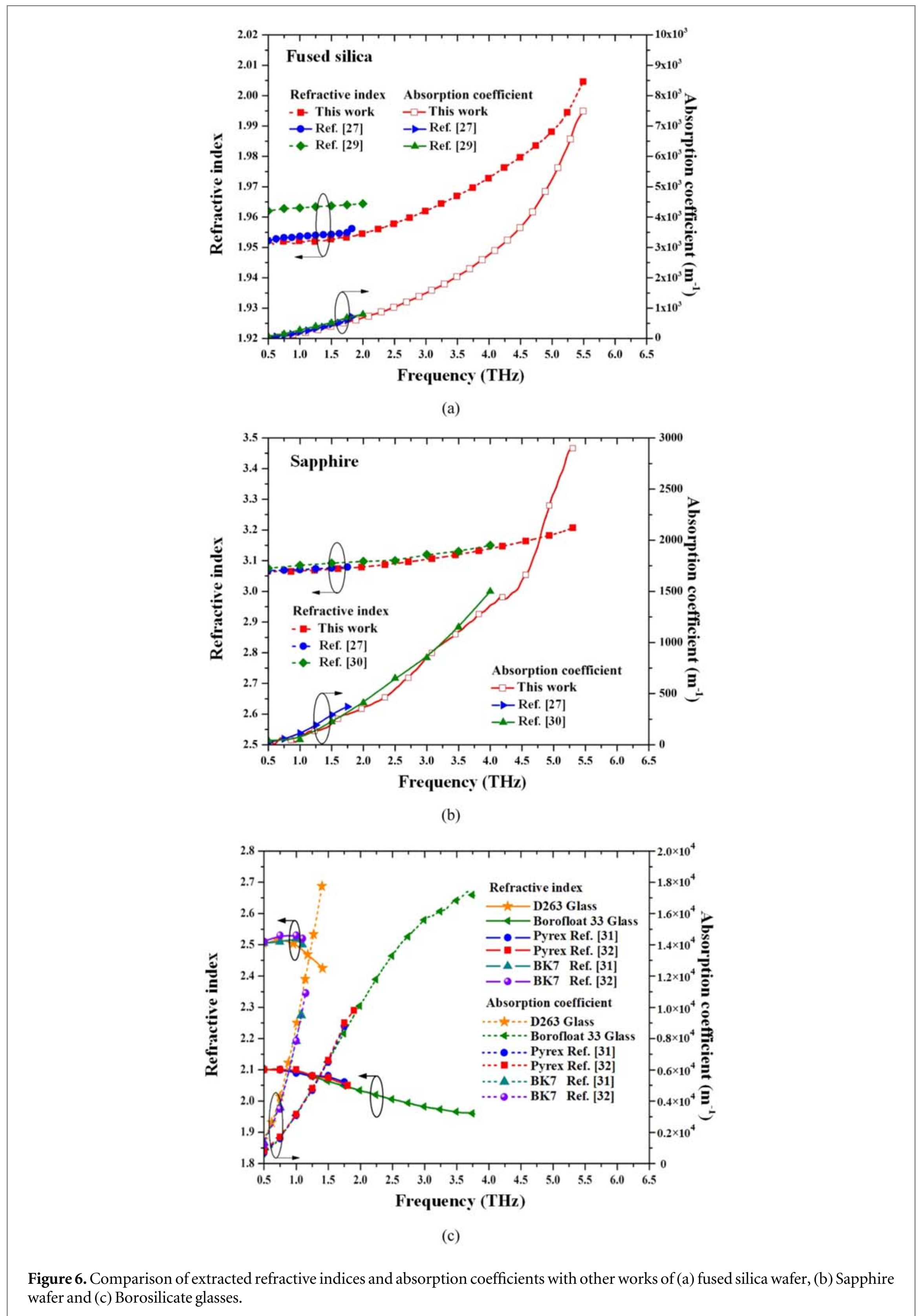

Figure 6. Comparison of extracted refractive indices and absorption coefficients with other works of (a) fused silica wafer, (b) Sapphire wafer and (c) Borosilicate glasses.

calculated and listed in tables 2–5. To confirm the fitting function, all the fitted data are plotted to compare with the raw measured data in figures 2–5. The fitted values show a good agreement in optical and electrical dielectric properties of high than 93% compared to raw measured results.

3.6. Comparison results with other works

A comparison of the extracted refractive indices and absorption coefficient are shown in figure 6. Figure 6 (a) depicts the comparison of the refractive index and absorption coefficient of fused silica. The refractive indices

Table 6. Refractive index comparison of this work and other works.

	Refractive index						
	Frequency (THz)						
Wafer material	0.5	1.5	2.5	3.5	4.5	5.5	6.5
Si (0.001-0.005 Ω-cm)	6.233	3.763	2.952	2.522	2.183	1.862	—
Si (0.01 – 0.02 Ω-cm)	5.227	3.689	3.298	3.075	2.848	@5.0THz 2.792	—
D263 glass	2.505	@1.4THz 2.424	—	—	—	—	—
Borofloat 33 glass	2.102	2.063	2.005	1.965	@ 3.8 THz 1.958	—	—
Fused Silica	1.952	1.925	1.957	1.967	1.979	2.005	—
Sapphire	3.065	3.072	3.090	3.120	3.160	@5.3THz 3.207	—
[27] Fused silica	1.952	1.954	—	—	—	—	—
[29] Fused silica	1.962	1.963	—	—	—	—	—
[27] Sapphire	3.067	3.075	—	—	—	—	—
[30] Sapphire	3.075	3.092	3.1	3.13	—	—	—
[31] Pyrex	2.1	2.08	—	—	—	—	—
[32] Pyrex	2.1	2.075	—	—	—	—	—
[31] BK7	2.505	—	—	—	—	—	—
[32] BK7	2.51	—	—	—	—	—	—

Table 7. Absorption coefficient comparison of this work and other works.

	Absorption coefficient (m^{-1})						
	Frequency (THz)						
Wafer material	0.5	1.5	2.5	3.5	4.5	5.5	6.5
Si (0.001-0.005 Ω-cm)	3.67×10^4	9.83×10^4	14.43×10^4	18.24×10^4	21.27×10^4	23.13×10^4	—
Si (0.01 – 0.02 Ω-cm)	2.61×10^4	5.24×10^4	7.57×10^4	10.10×10^4	11.45×10^4	@ 5.0 THz 13.30×10^4	—
D263 glass	1.61×10^3	@ 1.4 THz 1.81×10^4	—	—	—	—	—
Borofloat 33 glass	0.682×10^3	0.657×10^4	1.33×10^4	1.68×10^4	@ 3.8 THz 1.71×10^4	—	—
Fused Silica	9	418	1.05×10^3	2.07×10^3	3.71×10^3	7.53×10^3	—
Sapphire	12	207	544	1.10×10^3	1.60×10^3	@ 5.3 THz 2.90×10^3	—
[27] Fused silica	35	463	—	—	—	—	—
[29] Fused silica	75	520	—	—	—	—	—
[27] Sapphire	21.7	292.25	—	—	—	—	—
[30] Sapphire	42.42	225	650	1,150	—	—	—
[31] Pyrex	700	6.50×10^3	—	—	—	—	—
[32] Pyrex	800	6.60×10^3	—	—	—	—	—
[31] BK7	1.35×10^3	—	—	—	—	—	—
[32] BK7	1.20×10^3	—	—	—	—	—	—

presented in [27] and [29] are plotted over the frequency range of up to 1.75 THz and 2 THz, respectively. The refractive indices at 1.75 THz of [27, 29], and this work are 1.955, 1.964, and 1.952, respectively. The maximum difference of refractive index value between this work and [29] is 0.012. Three absorption coefficients (i.e., [27, 29], and this work) at 1.75 THz are 605 m^{-1}, 685 m^{-1}, and 533.18 m^{-1}, respectively. The variation of the three absorption coefficients shows a similar trend, increasing at the higher frequency. In figure 6 (b), the refractive index and absorption coefficient of Sapphire are plotted. The maximum frequency of the data reported in [27] and [30] is 1.75 THz and 4 THz, respectively. At 1.75 THz, the refractive indices of [27, 30], and this work are 3.079, 3.095, and 3.075, respectively. The maximum percentage difference of refractive indices of Sapphire between [30] and this work is 0.65%. The absorption coefficients of [27, 30], and this work at 1.75 THz are 372 m^{-1}, 330 m^{-1}, and 297.57 m^{-1}, respectively. Three absorption coefficients show the same tendency, such that the value of absorption coefficient increases at higher frequency. The refractive index (i.e., the solid line

Table 8. Dielectric constant comparison of this work and other works.

	Dielectric constant						
	Frequency (THz)						
Wafer material	0.5	1.5	2.5	3.5	4.5	5.5	6.5
Si (0.001-0.005 Ω-cm)	17.735	7.919	2.360	1.574	1.079	1.005	—
Si (0.01 – 0.02 Ω-cm)	14.312	4.506	6.679	5.633	4.990	@5.0THz 5.099	—
D263 glass	6.273	@1.4THz 5.786	—	—	—	—	—
Borofloat 33 glass	4.419	4.246	4.004	3.848	@3.8THz 3.823	—	—
Fused Silica	3.811	3.813	3.833	3.869	3.919	4.019	—
Sapphire	9.394	9.436	9.553	9.735	9.991	@5.3THz 10.287	—

Table 9. Loss tangent comparison of this work and other works.

	Loss tangent						
	Frequency (THz)						
Wafer material	0.5	1.5	2.5	3.5	4.5	5.5	6.5
Si (0.001-0.005 Ω-cm)	1.443	2.710	3.485	4.125	4.752	5.455	—
Si (0.01 – 0.02 Ω-cm)	1.069	0.815	0.704	0.766	0.705	@ 5.0 THz 0.680	—
D263 glass	0.059	@ 1.4 THz 0.255	—	—	—	—	—
Borofloat 33 glass	0.031	0.101	0.127	0.117	@ 3.8THz 0.110	—	—
Fused Silica	0.042×10^{-3}	0.006	0.010	0.014	0.019	0.032	—
Sapphire	0.045×10^{-3}	0.002	0.003	0.004	0.005	@ 5.3 THz 8.14×10^{-3}	—

with the indicated symbol) and absorption coefficient (i.e., the dashed line with symbol) of four borosilicate glasses (D263, Borofloat 33, Pyrex, and BK7) are illustrated in figure 6 (c). The Pyrex and BK7 used in [31, 32] are a type of borosilicate glass, which are compared with the D263 and Borofloat 33 glass in this work. The trend of the D263 glass is similar to that trend of BK7. Specifically, the maximum refractive index is 2.53 at 1 THz. Above 1 THz, the value of the refractive index of D263 glass is slightly reduced to 2.42 at 1.4 THz. On the other hand, the trend of the Borofloat 33 glass is similar to Pyrex, such that the value of the refractive index is lower when the frequency increases. In [31, 32], the maximum frequency of the data for Pyrex is 1.75 THz and 1.8 THz, respectively. Additionally, in this work, the refractive index of Borofloat 33 glass is expanded to 4.0 THz, and the value of Borofloat 33 glass slightly decreases between 2.102 and 1.958 from 0.5–3.8 THz. For the absorption coefficient of the borosilicate group, the extracted results of D263 and Borofloat 33 glass show good agreement when compared with BK7 and Pyrex, respectively. At the higher frequency, the values of the absorption coefficients of borosilicate glasses increase. To summarize the results of the comparison data and this work, the optical and electrical properties (e.g., refractive index, absorption coefficient, dielectric constant, and loss tangent) are listed in tables 6–9, respectively, which can be found in the appendix.

4. Conclusions

The optical and electrical properties of six selected wafers were characterized for their optical and electrical properties by using THz time-domain spectroscopy. The transmission method was used to measure the four wafers of D263 glass, Borofloat 33 glass, Fused silica and Sapphire. The reflection method was used to characterize the silicon wafers with low resistivity of 0.01-0.02 Ω-cm and 0.001-0.005 Ω-cm. The measurement results were presented from a low frequency of 0.5 THz to the highest frequency of 6.5 THz. To assess the accuracy and the reliability of the measurement results, the measured and extracted results have been compared with other published works of note and excellent agreement has been observed.

Acknowledgments

This work was supported funded by Thailand Science Research and Innovation Fund, and King Mongkut's University of Technology North Bangkok with contract no. KMUTNB-BasicR-64-39, and in part by the Engineering and Physical Sciences Research Council under Grant EP/S016813/1 and Grant EP/N010523/1.

Data availability statement

No new data were created or analysed in this study.

Appendix

The optical and electrical properties (e.g., refractive index, absorption coefficient, dielectric constant, and loss tangent) of the other published works [27 29–32] and this work are listed in tables 6–9, respectively.

ORCID iDs

Nonchanutt Chudpooti https://orcid.org/0000-0002-7239-9968

Nattapong Duangrit https://orcid.org/0000-0003-2617-8627

Andrew D Burnett https://orcid.org/0000-0003-2175-1893

Chuwong Phongcharoenpanich https://orcid.org/0000-0002-2057-3127

Ulrik Imberg https://orcid.org/0000-0002-5936-1260
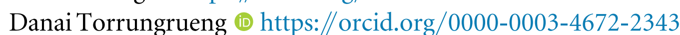
Danai Torrungrueng https://orcid.org/0000-0003-4672-2343

Prayoot Akkaraekthalin https://orcid.org/0000-0001-6520-0765

Ian D Robertson https://orcid.org/0000-0003-1522-2071

Nutapong Somjit https://orcid.org/0000-0003-1981-2618

References

[1] Nagatsuma T, Ducournau G and Renaud C 2016 Advance in terahertz communications accelerated by photonics *Nat. Photonics* **10** 371–9
[2] Koening S *et al* 2013 Wireless sub-THz communication system with high data rate *Nat. Photonics* **7** 977–81
[3] Han R *et al* 2019 Filling the gap *IEEE Microwave Mag.* **20** 80–93
[4] Robertson I, Somjit N and Chongcheawchamnan M 2016 *Microwave and Millimeter-Wave Design for Wireless Communications* 1st ed (New York: Wiley)
[5] Guerboukha H, Nallappan K and Skorobogatiy M 2018 Toward real-time terahertz imaging *Adv. Opt. Photonics* **10** 843–938
[6] Abina A *et al* 2015 Applications of terahertz spectroscopy in the field of construction and building materials *Applied Spectroscopy Review* **50** 297–303
[7] Han H, Yuan J and Tong J 2015 Design of THz applications system *J. Comput. and Commun.* **3** 61–5
[8] Choudhury B, Sonde A R and Jha R M 2016 Terahertz antenna technology for space applications, Terahertz Antenna Technology for space applications *SpringerBriefs in Electrical and Computer Engineering.* (Singapore: Springer)
[9] Lan F *et al* 2019 Dual-band refractometric terahertz biosensing with intense wave-matter-overlap microfluidic channel *Biochemical Optics Express* **10** 3789–99
[10] Lee D-K *et al* 2017 Nano metamaterials for ultrasensitive terahertz biosensing *Sci. Rep.* **7** 8146
[11] Breed G 2006 A comparison of RFIC fabrication technologies *High Frequency Electronics* 52–3 http://www.summittechmedia.com/highfreqelec/Mar06/HFE0306_Tutorial.pdf
[12] May J W and Rebeiz G M 2010 Design and characterization of *W*-band SiGe RFICs for passive millimeter-wave imaging *IEEE Trans. Microw. Theory Tech.* **58** 1420–30
[13] Shah U *et al* 2016 Submillimeter-wave 3.3-bit RF MEMS phase shifter integrated in micromachined waveguide *IEEE Trans. Terahertz Sci. Technol.* **6** 706–15
[14] Shah U *et al* 2017 A 500-750 GHz RF MEMs waveguide switch *IEEE Trans. Terahertz Sci. Technol.* **7** 326–34
[15] Hu Z, Wang C and Han R 2019 A 32-unit 240-GHz heterodyne receiver array in 65-nm CMOS with array-wide phase locking *IEEE J. Solid-State Circuits* **54** 1216–27
[16] Song H-J 2017 Packages for terahertz electronics *Proc. IEEE* **105** 1121–38
[17] Barker N S, Bauwens M, Lichtenberger A and Weikle R 2017 Silicon-on-insulator substrates as a micromachining platform for advanced terahertz circuits *Proc. IEEE* **105** 1105–20
[18] Ma Z T *et al* 2019 Modulators for terahertz communication: the current state of the art *Research* **2019** 6482975
[19] Božanić M and Sinha S 2019 Integrated substrates: millimeter-wave transistor technologies *Systems-Level Packaging for Millimeter-Wave Transceivers. Smart Sensors, Measurement and Instrumentation* (Berlin: Springer) 34, 105–28
[20] Inac O *et al* 2011 Millimeter-wave and THz circuits in 45-nm SOI CMOS *2011 IEEE Compound Semiconductor Integrated Circuit Symp. (CSICS) (Waikoloa, USA)*
[21] Schmalz N *et al* 2016 200–280 GHz CMOS RF front-end of transmitter for rotational spectroscopy *Proc. Symposia VLSI Technology and Circuits*
[22] Cheema H M and Shamim A 2013 The last barrier: on-chip antenna *IEEE Microwave Mag.* **14** 79–91

[23] Benaissa K *et al* 2003 RF CMOS on high-resistivity substrate for system-on-chip applications *IEEE Electron Device* **50** 567–75

[24] Park J-D *et al* 2012 A 260 GHz fully integrated CMOS transceiver for wireless Chip-to-Chip communication *Proc. IEEE Symp. on VLSI Circuits Technical Digest*

[25] Park J-D, Kang S and Niknejad A M 2012 A 0.38 THz fully integrated transceiver utilizing a quadrature push-push harmonic circuitry in SiGe BiCMOS *IEEE J. Solid-State Circuits* **47** 2344–54

[26] Rong B *et al* 2004 Surface-passivated high-resistivity silicon substrates for RFICs *IEEE Electron Device Lett.* **25** 176–8

[27] Takahashi S *et al* 2017 Development of high frequency device using glass or fused silica with 3D integration *2017 IEEE 67th Electron. Compon. and Technol. Conf. (ECTC)* 759–63*(Florida, USA)*

[28] Grischkowsky D *et al* 1990 Far-infrared time-domain spectroscopy with terahertz beams of dielectrics and semiconductors *J. Opt. Soc. Am. B* **7** 2006–15

[29] Dai J, Zhang J, Zhang W and Grischkowsky D 2004 Terahertz time-domain spectroscopy characterization of the far-infrared absorption and index of refraction of high-resistivity, float-zone silicon *J. Opt. Soc. Am. B* **21** 1379–86

[30] Naftaly M and Miles R E 2007 Terahertz time-domain spectroscopy of silicate glasses and the relationship to material properties *J. Appl. Phys.* **102** 043517

[31] Lee Y-S 2009 *Principles of Terahertz Science and Technology* (Berlin: Springer)

[32] Naftaly M and Miles R E 2007 Terahertz time-domain spectroscopy for material characterization *Proc. IEEE* **95** 1658–65

[33] Bolivar P H *et al* 2003 Measurement of the dielectric constant and loss tangent of high dielectric-constant materials at terahertz frequencies *IEEE Trans. Microw. Theory Tech.* **51** 1062–6

[34] Zhu H-T and Wu K 2021 Complex permittivity measurement of dielectric substrate in sub-THz range *IEEE Trans. Terahertz Sci. Technol.* **11** 2–15

[35] Li D, Ling F and Yao J 2019 Investigation of optical tuning on the dielectric properties of $0.3Ba_{0.4}Sr_{0.6}TiO_{3-0.7}NdAlO_3$ ceramics in terahertz range *IEEE Trans. Terahertz Sci. Technol.* **9** 505–9

[36] Chang T *et al* 2020 Terahertz dielectric spectroscopy based thermal aging analysis of polypropylene *IEEE Trans. Terahertz Sci. Technol.* **10** 363–9

[37] Ruan X and Chan C H 2019 Terahertz free-space dielectric property measurements using time- and frequency-domain setups,' *Int. J. RF Microw. Comput. Aided Eng.* **29** e21839

[38] Zheng Y *et al* 2020 Doomed couple of diamond with terahertz frequency: hyperfine quality discrimination and complex dielectric responses of diamond in the terahertz waveband *ACS Applied Electronic Materials* **2** 1459–69

[39] Sahin S *et al* 2019 Dielectric properties of low-loss polymers for mmW and THz applications *J. Infrared Milli. Terahz. Waves* **40** 557–73

[40] Bacon D R *et al* 2016 Free-space terahertz radiation from a LT-GaAs-on quartz large-area photoconductive emitter *Opt. Express* **24** 26986–97

[41] Duangrit N *et al* 2019 Terahertz dielectric property characterization of photopolymers for additive manufacturing *IEEE Access* **7** 12339–47

[42] Valavanis A *et al* 2016 Diffuse-reflectance spectroscopy using a frequency-switchable terahertz quantum cascade laser *IEEE Trans. Terahertz Sci. Technol.* **6** 341–7

[43] Dean P *et al* 2014 Terahertz imaging using quantum cascade lasers-a review of systems and applications *J. Phys. D:Appl. Phys.* **47** 374008

[44] Han P Y and Zhang X-C 2001 Free-space coherent broadband terahertz time-domain spectroscopy *Meas. Sci. Technol.* **12** 1747–56

[45] Nashima S *et al* 2001 Measurement of optical properties of highly doped silicon by terahertz time domain reflection spectroscopy *Appl. Phys. Lett.* **79** 3923–5

[46] High-Power, Coherent Company 2016 *Industrial and Fiber Laser Solutions Provider for Materials Processing and Scientific Markets. [Online]* Available: https://edge.coherent.com/assets/pdf/COHR_Vitara_DS_0416revC_3.pdf

[47] Jin Y-S, Kim G-J and Jeon S-G 2006 Terahertz dielectric properties of polymers *J. Korean Phys. Soc.* **49** 513–7

[48] Afsar M N 1984 Dielectric measurements of millimeter-wave materials *IEEE Trans. Microw. Theory Techn., MTT* **32** 1598–609

[49] Mickan S P and Zhang X-C 2003 T-ray sensing and imaging *Int. J. High Speed Electron. Syst.* **13** 601–76

[50] Silicon wafers & other Semiconductor substrates in stock (Oct. 2018). Retrieved January 10, 2020, from https://order.universitywafer.com/default.aspx?cat=Silicon&fbclid=IwAR2uIgX_DkOqIl7tgR_GET5QeYGIx4FSo3JFcbmEd2PPvbRaHwp2J3vJGRQ

[51] Japsen P U and Fischer B M 2005 Dynamic range in terahertz time-domain transmission and reflection spectroscopy *Opt. Lett.* **30** 29–31

[52] Origin(Pro), Version 2017 *OriginLab Corporation* (MA, USA: Northampton)